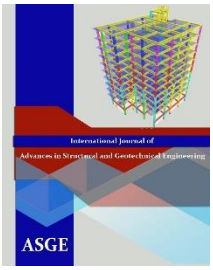

International Journal of Advances in Structural and Geotechnical Engineering

https://asge.journals.ekb.eg/

Print ISSN 2785-9509 *Online ISSN 2812-5142*

Special Issue for ICASGE'19

Behavior of tension lap splices in high-performance concrete using a new developed technique

Tarek Fawzy, Abdel-Hakim Khalil, Ahmed Atta, Hamdy M. Afefy, Mohamed Ellithy

ASGE Vol. 06 (02), pp. 1-19, 2022

International Conference on Advances in Structural and Geotechnical Engineering

ICASGE'21

29 March - 1 April 2021,Hurghada-Egypt

Behavior of tension lap splices in high-performance concrete using a new developed technique

Tarek Fawzy[1], Abdel-Hakim Khalil[2], Ahmed Atta[3], Hamdy M. Afefy[4], Mohamed Ellithy[5]

[1]*Professor of concrete structures, Faculty of Engineering, Tanta University, Egypt.*
E-mail: tarek.elshafi@f-eng.tanta.edu.eg

[2]*Professor of concrete structures, Faculty of Engineering, Tanta University, Egypt.*
E-mail: abdelhakeem.khalil@f-eng.tanta.edu.eg

[3]*Professor of concrete structures, Faculty of Engineering, Tanta University, Egypt.*
E-mail: Ahmed.Atta@f-eng.tanta.edu.eg

[4]*Professor of concrete structures, Faculty of Engineering, Tanta University, Egypt.*
E-mail: hamdy.afefy@f-eng.tanta.edu.eg

[5]*Assistant lecturer, Structural Engineering Department, Faculty of Engineering, Tanta University, Egypt.*
E-mail: mohamed.ezat@f-eng.tanta.edu.eg

ABSTRACT

An experimental and analytical study on seven specimens of lap splices embedded in high-performance concrete (HPC) prisms without confining reinforcement was performed under direct tension. The experimental program was classified into two groups; first group involved the straight-ended splices, while the second studied a new developed technique based on anchor-ended splices. For straight-ended bars, conventional lap splice was studied as a benchmark. The anchor-ended splices contained embedded steel plates connected to the ends of the spliced bars, by which the slippage of bars was suppressed. It was found that the used technique not only achieved higher capacity at failure, but also a bond induced failure was altered with a rupture of bars at its maximum tensile strength. Finally, an analytical model was proposed in order to predict the ultimate tensile stress of the straight-ended spliced bars. The accuracy of the proposed model was verified against the test results of 137 existing specimens from previous research. The comparison showed good agreement between the results of the proposed model and the test results.

Keywords: Lap splice, direct tension, anchor-ended, plate-ended.

1. INTRODUCTION

The overall structural performance of reinforced concrete elements is mainly dependent on the bond characteristics between reinforcing steel bars and the surrounding concrete. Therefore, the adopted development lengths and lap splices of reinforcing steel bars have to be fully understood. Thus, this area of research has attracted the interest of many researchers worldwide. The governing parameters have been found to be the concrete type/strength, reinforcing bar diameter, concrete cover, method of splicing of bars, confinement of bars, coating of bars and loading type.

Since the type of concrete is an effective parameter, using Ultra-High-Performance Fiber Reinforced Concrete (UHPFRC) showed a considerable improvement on bond performance and splitting crack control. For UHPFRC mix having fiber volumetric ratio of 4%, a splice length of 12 d_b was found to be sufficient for achieving yield for 400 MPa reinforcement [1]. Also, Strain-Hardening Cementitious Composite (SHCC) mixtures was found to be effective in reducing the development length of rebar up to 60 percent of the splice length required by the ACI 318 equation according to splitting failure controlled by multiple cracking behavior of SHCC mixtures [2]. Fiber Reinforced Cement Composites (FRCC) showed that the fibers induced bridging effect after cracking can effectively support post-cracking tensile capacity to the concrete matrix and limit crack width, thereby leading to enhanced bond resistance [2,3,4,5]. The effectiveness of UHPFRC for strengthening deficient lap splices was tested in 18 full-scale beam specimens. Splitting failure in the lap splice region was completely eliminated due to the high tensile strength and energy absorption capabilities of the used UHPFRC [6]. Furthermore, splice length of deformed bars embedded into high-strength self-compacted concrete beams were examined [7]. A splice length of 40 times bar diameter was found the minimum splice length to be taken as a sufficient splice length since beams started cracking and failed at a load equal or higher than those without splice [7]. Researches have also proved that the bond behavior and failure modes were noticed to be similar in the natural and the recycled aggregate concrete [8].

Regardless of concrete type, the failure of specimens with lap splices without transverse reinforcement was violent and occurred along the entire length of the splice. Adding proper confinement along the splice zone improved the behavior as the proper confinement eliminated the formation of splitting cracks at tension splice zone [9,10,11]. Several techniques were used in order to strengthen the ordinary lap splice such as welding, headed bars and hooks. The main idea of hooks and headed bars is to use anchors at the end of steel bars which provides higher resistance for reinforcing bars against slippage. Although welded splicing reduces rebar congestion and improves concrete consolidation, it requires special labor and equipment which entails additional coast [12]. Headed bars can transfer the bar full strength to concrete with only $4d_b$ splice length [13]. Therefore, headed bar could be

considered as an effective way to minimize the lap splice length but it still not practical method in narrow elements with adjacent lapped bars. Equations were developed to estimate the anchorage strength of hooked bars with and without confining reinforcement. The equations are based on test results of 245 simulated beam-column joint specimens [14].

Lap splice is considered the most economic and the easiest way for splicing the reinforcing steel bars. Accordingly, the current research is devoted to develop and study the behavior of a new developed technique for lap splices aiming to increase their capacity as well as minimizing the splice length.

2. EXPERIMENTAL INVESTIGATION

2.1 Test specimens and studied parameters

In the current study, the specimens are two pairs of lap spliced 12 mm diameter bars in HPC prism without transverse reinforcement and were axially loaded by tension force. The tested specimens were categorized into two different groups according to the configuration of the steel bars. Group 1 consisted of straight bars without transverse steel as depicted in Fig. 1, while Group 2 presented anchor-ended spliced bars without confining reinforcement. The steel bars of Group 2 were anchored using steel plates as shown in Figs. 2 and 3. Table 1 summarizes the concrete prism dimensions and lap lengths for each group.

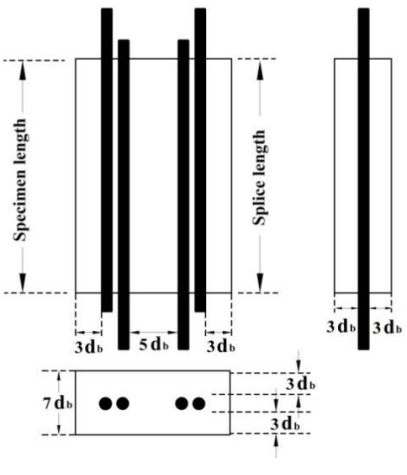

Fig. 1 Configuration of Group (1-O), ordinary lap splice.

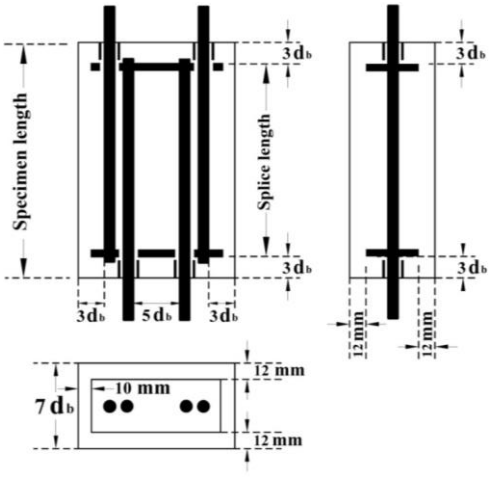

Fig. 2 Configuration of Group (2-P), end bearing plate.

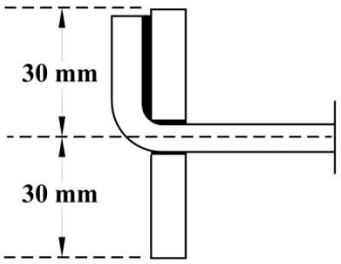

Fig. 3 Steel plate in which the bar is welded to the rear face.

Table 1 Specimens notations and dimension

Group	Splice length	Specimen notation	Prism dimensions (mm)		
			Length	Width	Depth
G1-O	10 d_b	G1-O-10d	120	180	84
	20 d_b	G1-O-20d	240	180	84
	30 d_b	G1-O-30d	360	180	84
G2-P	05 d_b	G2-P-05d	130	180	84
	10 d_b	G2-P-10d	190	180	84
	20 d_b	G2-P-20d	310	180	84
	30 d_b	G2-P-30d	430	180	84

The adopted notation system of specimens shows the various testing parameters; where for specimen Gx-y-zd, "x" indicates the group, "y" refers to the type of splice and "z" is the splice length in term of bar diameter. The back of the anchors was covered by concrete with length of $3d_b$, in this zone the bars were isolated to maintain the splice length between anchors. The configuration of specimens in the current study was adopted in several previous researches, which allows testing of full length lap splice without execution of full-scale beam splice specimen. The bond strength obtained by this configuration lays between 90% and 100% of what obtained by beam splice specimens with same conditions [1,15,16]. In this research the minimum concrete cover was deliberately selected $3d_b$ for all test specimens. The chosen concrete cover is common in practice in RC beams in the Middle East.

2.2 Steel bars properties

The nominal yield strength of reinforcing bars was 400 MPa as typically used in the Middle East. For each bar diameter, three samples were collected and tested in accordance with ASTM A370 [17]. The average mechanical properties and geometries of the tested samples are listed in Table 2.

Table 2 Steel bars geometries and mechanical properties

Property	Splice bar
Nominal diameter, d_b (mm)	12
Core diameter, D (mm)	12
Average rib depth, h_r (mm)	0.9
Rib spacing, s_r (mm)	8.5
Rib face angle, ɵ (^{O})	37
Relative rib area, R_r	0.1125
A_b (mm^2)	114.7
Young modulus, Es (GPa)	207
Yield strength, f_y (MPa)	463
Ultimate strength, f_u (MPa)	631

2.3 HPC material properties

The HPC mix was the same for all tested specimens, the mix shows a self-consolidating behavior allowing an excellent workability with light vibration. The concrete mix performed in the current research was the same mix used in a previous research [18]. The concrete mix is summarized in Table 3 where the water-to-cement ratio was 0.3. Precautions were taken to ensure bars alignment among the wood forms during casting. The current HPC mix showed well consolidation and was poured with light vibration. After casting, specimens were covered by wet textile then curing process began and continued for six days. Material tests of HPC were performed at the same day of the lap splice test.

Table 3 Concrete mix design of HPC (kg/m^3)

Cement	Water	Sand	Dolomite	Silica fume	Super plasticizer	Polypropylene fibers
450	135	535	1279	45	4.5	1.8

Compressive strength f_c' was determined from 150 x 300 mm standard cylinders according to ASTM C39 [19]. Brazilian test was performed to obtain the tensile strength f_t of HPC. Two cylindrical samples for each group were tested to determine the compressive and tensile strengths at the day of testing the splice specimens of the same group. To ensure early gained strength, one cylinder sample was tested, the 7 days age compressive strength was 40.1 MPa. Table 4 reports HPC main characteristics regarding to each group.

Table 4 HPC material properties

Group	f_c' (MPa)	f_t (MPa)
G1-O	54	4.7
G2-P	58	5.1

2.4 Instrumentation

One strain gauge outside the specimen for each lap splice bar was mounted to determine the strain in each bar during the test. A total of 4 LVDT (Linear Variable Differential Transformer) with a 50 mm gauge length were installed on the concrete surface at $4d_b$ from each end on the specimen front faces, perpendicularly to the axis of the splice joint as depicted in Fig. 4. The faces were sprayed with white color to have a clearer view of the cracks took place on the surface of the specimens. MTS actuator was used to apply tension force and its outputs (load-displacement) were recorded. The failure of specimens is sudden and violent, thus, tests were recorded by slow-motion HD video camera with 120 fbs.

2.5 Test setup

Splice bars were fixed to a rigid steel cap system via steel grips and wedges to ensure that both lapped bars were subjected to the same displacement. The rigid capping system was tested against bare bars, the cap deformation was inferior to 0.3 mm. To assure the best fitting of the bars with grips, the specimens were preloaded to 5 kN then released before testing. The rigid cap was attached to the thick platen of MTS actuator. Loading was applied by force control of the two top bars with a constant load rate 5 kN/min until failure. During the test, actuator output

data was exported to a data-logger with sampling frequency 2 Hz. Fig. 4 presents the specimen, the instrumentation and the experimental set-up.

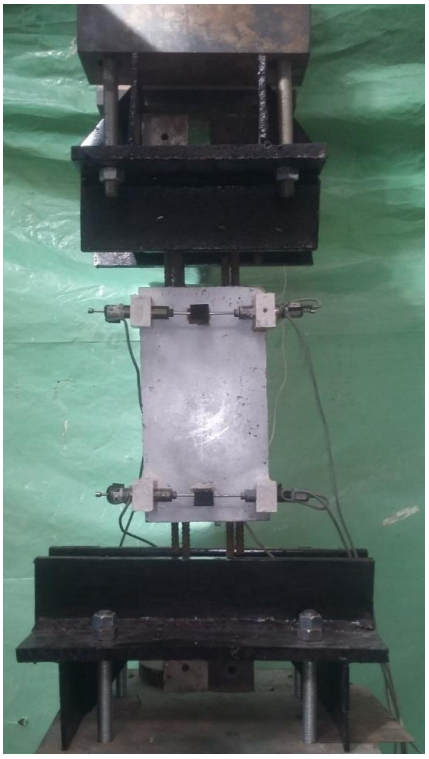

Fig.4 Test setup and instrumentation.

3. RESULTS AND DISCUSSION

3.1 Overall behavior

Test results at maximum load for all tested lap splice specimens are summarized in Table 5. The maximum steel stress at failure f_s represents the average stress developed at the reinforcing bars. Bars stress is the output of dividing the maximum force by the average cross section of steel bars. Weight and length measurements were used to calculate the average cross section A_b of steel bars as shown in Table

2. The maximum steel stress was compared to the actual yield strength of steel in term of f_s / f_y to calculate the efficiency of splice E_f.

Table 5 Test results of lap splice specimens

Group	Specimen notation	Max. Load (kN)	f_s (MPa)	E_f (f_s /f_y)	Mode of failure
G1-O	G1-O-10d	60.9	265	0.58	P
	G1-O-20d	118.7	517	1.12	YP
	G1-O-30d	132.1	576	1.25	YP
G2-P	G2-P-05d	145.5	634	1.37	R
	G2-P-10d	145.2	633	1.37	R
	G2-P-20d	138.6	604	1.30	R
	G2-P-30d	142.4	621	1.34	R

P : Pullout/slippage of reinforcing bars.
YP : Yielding of steel followed by pullout/slippage of bars.
R : Rapture of reinforcing bars.

Table 5 presents the test outputs and the exhibited modes of failure. Straight-ended splices with lengths of 10, 20 and 30d_b reached a tensile stress of 265, 517 and 576 MPa, respectively. Although splice length of 10d_b did not achieve the yield stress, the other specimens of straight-ended splices exceeded the yield stress of steel bars. For specimens of G1-O with splice length 10, 20 and 30d_b, the maximum developed bond stress is 6.71, 6.55 and 4.86 MPa, respectively. G1-O-30d exhibited an obvious lower value of the developed maximum bond stress comparing with the other specimens of G1-O. This is attributed to the effect of non-uniform bond stress distribution along the splice length. It is clear that the new developed anchoring technique of plate-ended splices raised their capacities than those of the straight-ended. All specimens of G2-P achieved the maximum potential strength of steel and rupture of reinforcing bars took place.

3.2 Mode of failure

Shear crack and/or local concrete crushing due to bar pullout was noted for all specimens of G1-O as shown in Fig. 5. The failure of G1-O-10d was prior to yielding of steel bars and the other specimens of G1-O failed after yielding. Splitting cracks were not obvious during testing and appeared only simultaneous with failure. Developing an innovative technique of end bearing plate for G2-P leaded to the same mode of failure for all anchored specimens. The specimens of G2-P showed rapture of reinforcing bars with maximum potential strength of steel. During testing of G2-P specimens, the movable plates converted the tension force of bars into compression force acting between the plates. This action played a role of suppressing the tensile

cracks of concrete during testing especially in short lap splice specimens G2-P-5d and G2-P-10d which remained without cracking until failure. Fig. 6-a shows the rupture of steel bar of specimen G2-P-10d, while, Fig. 6-b shows the compression force created on the face of bearing plates.

Fig. 5 Bars pullout of G1-O-20d.

(a) Rupture of reinforcing steel bars of for S-P-05d.

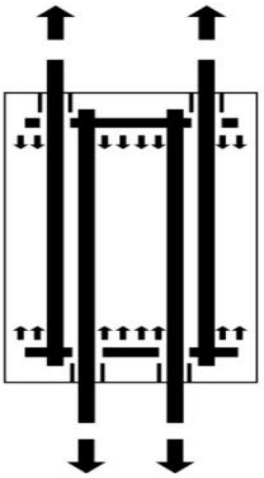

(b) Compression force acting between plates.

Fig. 6 failure characteristics and force transfer of anchor-ended specimen.

3.3 Bond-slip response

The bar-to-concrete relative slip at bar's free end for straight-ended specimens were recorded during the test. Subsequently, the relationship between the bond-stress vs. relative slip at the bar's free end was plotted. Fig. 7 shows the bond vs. slip curves for straight-ended specimens. Generally, it was observed that the bond stress of sub-group G1-O where all specimens failed due to bars pullout showed an obvious drop after the peak stress. This is caused by the absence of confining reinforcement which plays a role in equilibrating the bursting forces caused by the bond action. While, a minor portion of bond strength induced by tension stiffening of concrete is maintained owing to the fact that the tensile strength of concrete does not be lost instantly after cracking. It was clearly obvious that specimens of splice lengths of 10 and 20d_b approximately exhibited a close behavior, on the other hand, the splice of 30d_b length showed a different behavior. This is caused by the effect of the non-uniformly distributed bond stress within the splice which becomes more obvious as long as the splice length is longer.

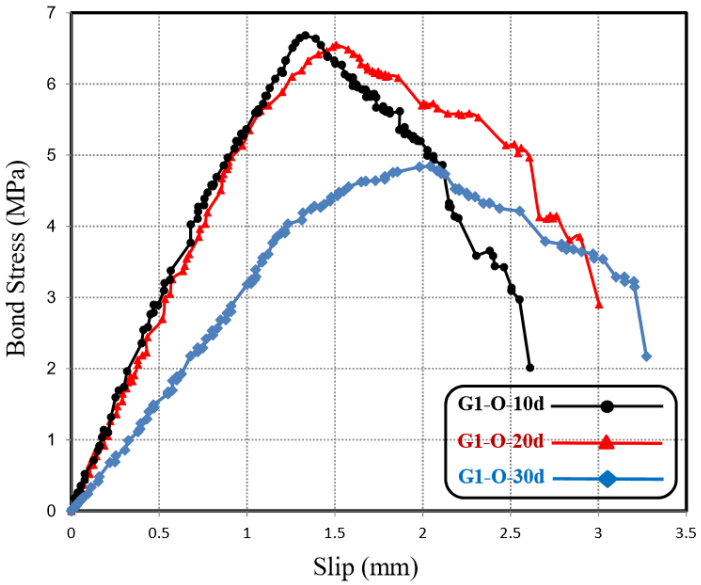

Fig. 7 Bond-slip relationship for specimens of G1-O.

4. Analytical study

Codes and design provisions consider a uniform bond stress distribution along developed/spliced reinforcing bars. This may underestimate the bond strength gained by long development/splice lengths. Based on the non-uniform bond stress distribution for elastic bars, Hwang et al. [20] established an analytical model to predict the maximum tensile stress of spliced/developed bars. In order to overcome the yielding of steel bars, Hwang et al. [20] considered that the maximum estimated tensile strength of a bar does not exceed the yield stress, thus, Hwang' model cannot be judged in terms of overestimating the bond strength. In the current study, a new proposed model was developed taking into consideration the state of the yielded bars. Comparisons were carried out between the predicted and the experimental results of 137 existing splice specimens to validate the proposed model.

4.1 Proposed model for predicting the ultimate tensile stress of straight-ended spliced bars

Based on the non-uniform bond stress distribution [20], a simplified bond stress distribution along an embedded length (*L*) of a steel bar under tensile pullout force (*P*) is shown in Fig. 8.

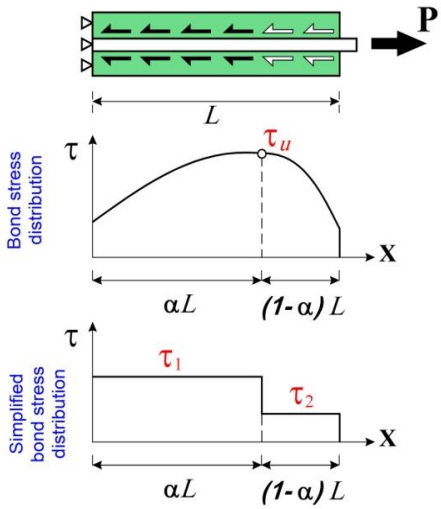

Fig. 8 Simplified bond stress distribution along the bar length.

Using the ratio (α), the embedded length is divided into two zones (the loaded/unloaded zones). At the bar's loaded end $(x = \alpha L \rightarrow x = L)$, the relative deformation exceeds the deformation related to the maximum bond stress, which refers to a local bond damage leading to a reduction in bond stress near to the loaded end. In the unloaded embedded part of the bar $(x = 0 \rightarrow x = \alpha L)$, as long as the relative deformation rises, the bond stress increases. The peak bond strength (τ_u) and the accompanied slip (S_1) are defined as follows [21]:

$$\tau_u = 0.91\,\alpha_d \sqrt{f_c'} \quad (in\ MPa) \qquad (1)$$

$$S_1 = 0.30 \sqrt{f_c'/30} \quad (in\ MPa\ and\ mm) \qquad (2)$$

Where; α_d = the bar's diameter coefficient; (1.1 for $d_b \leq 19$ mm, 1.0 for $22 \leq d_b \leq 29$ mm and 0.9 for $d_b \geq 32$ mm); f_c' = standard cylinder compressive strength. According to previous research, the bond stress affected by the yielding of bars at the loaded end which known as yield penetration [22]. The bond stress at the damaged region becomes less than that in the case of elastic bar; consequently, the lab splices with lengths exceed $20d_b$ did not reach a significant gain in capacity than that of the shorter splices [22]. The distribution of bond stress is dependent on the equation of deformation which relies on the bar's strain. On the other hand, the tensile strain distribution at the damaged part will be affected due to the decrease in the modulus of elasticity at the yielded part. In the current proposed model, for simplicity, the stress-strain relationship of steel can be considered as a bilinear relationship. In bilinear stress-strain relationship, after yielding stress, the value of young's modulus can be defined as the inclination of the line between the yielding point and the ultimate strength point. The young's modulus after yield point (E_P) can be assumed as 0.02 of the elastic modulus (E_S). Subsequently, the bar's strain relationship in the damaged region of the bonded length will be affected as shown in Fig. 9. At the plastic stage of the steel bar, the stress and strain of the bar are not linearly proportional but the bilinear stress-strain relationship can be applied. Thus, the following equations describe the strain at any point located at distance *x* along the damaged/undamaged regions.

The strain of the undamaged zone is ε_1 and the strain of the damaged zone is ε_2. For bars that do not reach the tensile yield stress, the young's modulus of plastic behavior (E_P) will be replaced by (E_S) in Eq. (4).

$$\varepsilon_1 = \frac{4\,\tau_1\,x}{E_s\,d_b} \quad \Rightarrow \quad (0 \rightarrow \alpha L) \qquad (3)$$

$$\varepsilon_2 = \frac{4\,\tau_1\,\alpha L}{E_s\,d_b} + \frac{4\,\tau_2\,(x-\alpha L)}{E_p\,d_b} \Rightarrow (\alpha L \rightarrow L) \qquad (4)$$

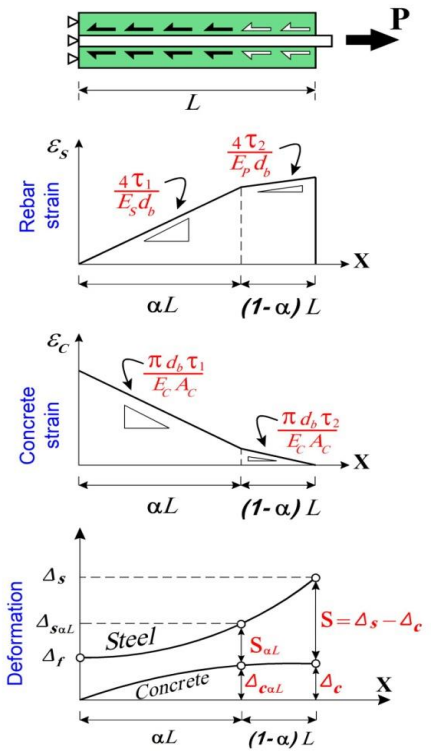

Fig. 9 Concrete/steel strain distribution along the bar length.

As shown in Fig. 9, the absolute deformation of reinforcing bar (Δ_S) along X axis can be estimated by integrating the strain equations as following:

$$\begin{aligned}\Delta_S &= \Delta_f + \int_0^{\alpha L} \varepsilon_1 \, dx + \int_{\alpha L}^{L} \varepsilon_2 \, dx \\ &= \Delta_f + \left| \frac{4\,\tau_1\,x^2}{2\,E_s\,d_b} \right|_0^{\alpha L} + \left| \frac{4\,\tau_1\,\alpha\,L\,x}{E_s\,d_b} + \frac{4\,\tau_2\,x^2}{E_p\,d_b} - \frac{4\,\tau_2\,\alpha\,L\,x}{E_p\,d_b} \right|_{\alpha L}^{L} \\ &= \Delta_f + \frac{L^2}{d_b\,E_s}(4\alpha - 2\alpha^2)\,\tau_1 + \frac{L^2}{d_b\,E_p}(2 - 4\alpha + 2\alpha^2)\,\tau_2\end{aligned} \qquad (5)$$

Where Δ_f is the absolute deformation of the steel bar at zero strain (*x =0*).

The relative displacement at $(x = \alpha\ L)$ where the maximum bond stress ($S_{\alpha L}$= S_1) can be expressed by subtracting the absolute deformations of steel ($\Delta_{S\alpha L}$) and concrete ($\Delta_{C\alpha L}$) as follows:

$$\begin{aligned} S_{\alpha\ L} &= S_1 = \Delta_{S\alpha L} - \Delta_{C\alpha L} \\ &= \Delta_f + \int_0^{\alpha L} \varepsilon_1\ dx - \Delta_{C\alpha L} \\ &= \Delta_f + \left| \frac{4\ \tau_1\ x^2}{2 d_b\ E_s} \right|_0^{\alpha L} - \Delta_{C\alpha L} \\ &= \Delta_f + \frac{L^2}{d_b\ E_s} \left(2\alpha^2 \tau_1\right) - \Delta_{C\alpha L} \end{aligned} \qquad (6)$$

Owing to the effect of the defected bond strength, the difference between the concrete strains and accordingly deformations at (x=αL) and at (x=L) is negligible. Therefore, to simplify the equations, the values of $\Delta_{C\alpha L}$ and Δ_C was assumed to be equal. Then the relative displacement (S) at the end of the bar (x=L) can be obtained as follows:

$$S = S_1 + \frac{L^2}{d_b\ E_s}(4\alpha - 4\alpha^2)\tau_1 + \frac{L^2}{d_b\ E_p}(2 - 4\alpha + 2\alpha^2)\tau_2 \qquad (7)$$

Considering

$$C_1 = \frac{L^2}{d_b\ E_s\ (1 - S_1)} \quad \& \quad C_2 = \frac{L^2}{d_b\ E_p\ (1 - S_1)}$$

The term (τ_2) can be expressed as a function of (τ_1) and (τ_u) as follows:

$$\tau_2 = \frac{1 - 2\ C_1 \alpha (1 - \alpha)\tau_1}{1/\tau_u + C_2 (1 - \alpha)^2} \geq \frac{\tau_u}{2} \qquad (8)$$

The bond stress (τ_1) can be expressed as follows [21]:

$$\tau_1 = \frac{1}{S_1 - \Delta_f} \int_{\Delta_f}^{S_1} \tau_u \left(\frac{S}{S_1}\right)^{0.40} ds \quad = \frac{\tau_u}{1.40} \times \frac{1 - \left(\Delta_f / S_1\right)^{1.40}}{1 - \left(\Delta_f / S_1\right)} \leq \tau_u \qquad (9)$$

From Eq. (6), by dividing the equation by S_1, the term Δ_f/S_1 can be expressed as follows:

$$\Delta_f \Big/ S_1 = 1 - \frac{L^2}{d_b\, S_1\, E_s}\left(2\alpha^2\tau_1\right) + \frac{\Delta_C}{S_1} \;\geq 0 \qquad (10)$$

Finally, the ultimate tensile stress (f_s) of the steel bar under pullout force can be expressed as given in Eq. (11):

$$f_s = \frac{4L}{d_b}\left[\alpha\tau_1 + (1-\alpha)\tau_2\right] \;\Rightarrow\; (f_y \leq f_s \leq f_u) \qquad (11)$$

Where f_y and f_u are the yield and ultimate strengths of the embedded steel bar, respectively. For cases at which the bars do not attain the tensile yield stress, the term "C_2" can be replaced by "C_1" in Eq. (8). Based on the test results collected from several researches, assumptions were made to limit the variations between the predicted and the experimental results. Statistical analysis were applied on the results of 137 tested specimens. It was found that the length ratio of undamaged part (α =0.75) gives the best predicted results comparing to the available test data. The concrete displacement (Δ_c) can be estimated by the definite integration of the concrete strain along the bonded length, which approximately equal to $\alpha L\varepsilon_c/2$, where ε_c is the maximum concrete strain at x =0. The concrete strain can be approximately considered as a constant value and equals to 0.001 [20].

4.1.1 Proposed model summary

In case of insufficient thickness of cover concrete and/or the confining reinforcement, the splitting failure takes place prematurely to pullout failure with a decrease in bond strength. The bond strength calculated by Eq. (3) was not considering the splitting failure, thus, the modification factor of ACI 408R-03 [23] is used to reduce the bond strength due to splitting failure and lack of transverse reinforcement.

$$\tau_u = 0.91\,\alpha_d\,\sqrt{f_c'}\left[\frac{(cw + k_{tr})/d_b}{2.5}\right] \quad (N \;\; and \;\; mm) \qquad (14)$$

Where; α_d = the bar's diameter coefficient; $c=c_{min}+0.50d_b$; $w=0.10(c_{max}/c_{min})+0.90 \leq 1.25$; $k_{tr} = \frac{A_{tr}\,C_R}{s\,n}(0.0283 d_b + 0.28)$ [23] ; $(cw + k_{tr})/d_b \leq 4.00$; C_R = 44+330 (R_r – 0.10); c_{min} = minimum [c_s , c_b]; c_{si} = 1/2 of the bar clear spacing; c_{so} = side concrete cover for reinforcing bar; c_s = minimum [c_{so} , c_{si} + 0.25 in.]; c_b = bottom concrete cover; c_{max} = maximum (c_b, c_s); A_{tr} = area of stirrups branches cross the splice zone; f_{yt} = yield strength of transverse reinforcement; s = spacing of transverse reinforcement; n = number of bars being developed or spliced; R_r = relative rib area of the reinforcement. In the short splices, the bond stress distribution along the

bonded length tends to be uniform and the unit length bond stress at failure (U_n) achieves an acceptable accuracy comparing to the bond strength (τ_u). For the application of the proposed model, the value of unit length bond stress at failure could be utilized instead of τ_u if it was provided by the experimental results of short spliced/developed bars.

4.1.2 Validation of the proposed model

The proposed model was applied to 137 existing specimens from previous research works. The specimens involve widely varied parameters, concrete cylinder compressive strengths (f_c') between 26 and 110 MPa, steel yield stress between 453 and 555 MPa, relative rib areas between 0.06 and 0.14, bars' diameters between 12 and 36 mm and splice lengths between 10 and $35d_b$. The experimental results of the current research in addition to the results of previous work were used to validate the proposed model. 83 beams splice specimens of Darwin et al. [24], 70 beams splice specimens of Azizinamimi et al. [25] and three direct tension splices of the current research were used. Nineteen beams splice specimens were eliminated from verification because they failed away of splice due to other reasons. As shown in Fig. 10, the data of the predicted (f_s) and the tested (f_{test}) tensile strengths of the 137 splice specimens were compared considering the splice length to bar diameter ratio (L_s/d_b). The average predicted to test results ratio was about 1.11 with standard deviation of about 0.151 and coefficient of variance (COV) of about 0.135. In the current research, the unit bond strength was obtained by the direct tension test of G1-O-05d, it was considered as 6.71 MPa. The model was applied to three specimens of sub-group G1-O. The predicted ultimate tensile stress of the bars was found in acceptable limits compared to the test results.

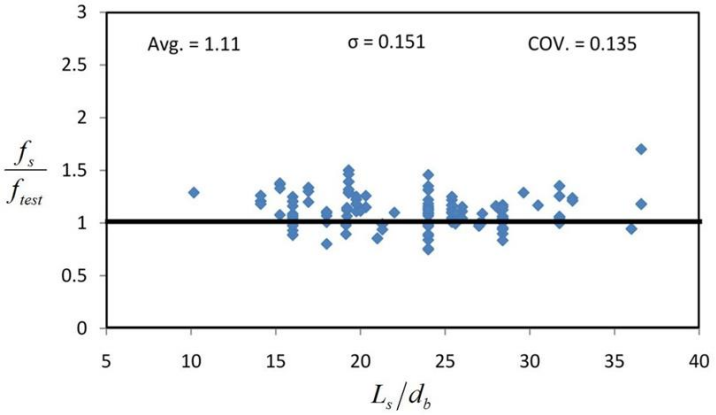

Fig. 10 Ultimate tensile predicted/test stress ratio of beam splice specimens.

5. Conclusions

The main objective of this paper was to experimentally investigate the new developed technique to enhance the splice strength in HPC prism under direct tension. The test specimens consisted of two pairs of spliced bars in a HPC prism without confining reinforcement. Four different splice lengths were performed to develop practical method to minimize the conventional lap splice. Based on the experimental outputs of the current study, the following notes can be concluded.

- All specimens of G1-O failed due to pullout of steel bars followed by concrete crushing and/or shear failure at different loading stages.
- The maximum developed bond stress at failure recorded by straight-ended specimens with splice lengths of 10 and $20d_b$ showed approximately similar values, while, the longer splice of $30d_b$ of splice length showed a lower value. This is attributed to the non-uniform bond stress distribution along the splice length.
- Rapture of reinforcing bars was attained by all specimens of G2-P with innovative technique of end bearing plates.
- Specimens G2-P-5d and G2-P-10d remained without cracking during testing owing to the action of plates which converted the tension force of bars into compression force acting on concrete in front of the plates.
- Based on the non-uniform stress distribution, a new model with modification of bond stress at the loaded end (τ_2) in case of yielded bars was proposed. The proposed model accuracy was verified against 137 existing specimens. The predicted to test results showed an acceptable variation.

ACKNOWLEDGEMENT

The experimental work was performed in the Reinforced Concrete and Heavy Structures Laboratory of Faculty of Engineering, Tanta University, Tanta, Egypt.

REFERENCES

[1] Lagier, F., Massicotte, B. and Charron, J., (2015), "Bond strength of tension lap splice specimens in UHPFRC", Construction and Building Materials Vol. 93, pp. 84–94.

[2] Choi, W., Jang, S. and Yun, H., (2016), " Bond and cracking behavior of lap-spliced reinforcing bars embedded in hybrid fiber reinforced strain-hardening cementitious composite (SHCC)", Composites Part B.

[3] Dagenais, M. and Massicotte, B., (2017), " Cyclic Behavior of Lap Splices Strengthened with Ultrahigh Performance Fiber-Reinforced Concrete", Structural Engineering, Vol. 143 (2).

[4] Marchand, P., Baby, F., Khadour, A., Battesti, T.,Rivillon, P., Quiertant, M., Nguyen, H.,Gre´goryGe´ne´reux, Deveaud, J., Simon, A., and Toutlemonde, F., (2016), "Bond behavior of reinforcing bars in UHPFRC", Materials and Structures, Vol. 49, pp. 1979–1995.

[5] Metelli, G., Marchina, E., Plizzari, G.A., (2017), "Experimental Study on Staggered Lapped Bars in Fiber Reinforced Concrete Beams", Composite Structures.

[6] Dagenais, M. and Massicotte, B., (2015), "Tension Lap Splices Strengthened with Ultrahigh-Performance Fiber-Reinforced Concrete", Materials in Civil Engineering, Vol. 27 (7).

[7] El-Azab, M., Mohamed, H. and Farahat, A., (2014), "Effect of tension lap splice on the behavior of high strength self-compacted concrete beams", Alexandria Engineering Journal.

[8] Prince, M., Gaurav, G. and Singh, B., (2018), "Splice strength of deformed steel bars embedded in recycled aggregate concrete", Construction and Building Materials, Vol. 160, pp. 156–168.

[9] Garcia, R., Helal, Y., Pilakoutas, K. and Guadagnini, M., (2014), "Bond behavior of substandard splices in RC beams externally confined with CFRP", Construction and Building Materials, Vol. 50, pp. 340–351.

[10] Hamad, B., Ali, A. and Harajli, M., (2005), "Effect of Fiber-Reinforced Polymer Confinement on Bond Strength of Reinforcement in Beam Anchorage Specimens", JOURNAL OF COMPOSITES FOR CONSTRUCTION, Vol. 9(1), pp. 44-51.

[11] Mabrouk, R. and Mounir, A., (2017), " Behavior of RC beams with tension lap splices confined with transverse reinforcement using different types of concrete under pure bending", Alexandria Engineering Journal.

[12] Issa, C.A. and Nasr, A., (2006), "An experimental study of welded splices of reinforcing bars", Building and Environment, Vol. 41, pp. 1394–1405.

[13] Vella, J. P., Vollum, R. L., and Jackson, A., (2017), " Investigation of headed bar joints between precast concrete panels", Engineering Structures, Vol. 138, pp. 351–366.

[14] Sperry, J., Darwin, D., O'Reilly, M., Lequesne, R. D., Yasso, S. Matamoros, A., Feldman, L. R. and Lepage, A., (2017), "Conventional and High-Strength Hooked Bars— Part 2: Data Analysis", ACI Structural Journal, Vol.114, No.1, pp.267-276.

[15] Burkhardt, C., (2000), "Behavior of lap splices in high strength concrete", [Ph.D thesis], Aachen, Germany: RWTH Aachen University; p. 190 [in German].

[16] Richter, B., (2012), "A new perspective on the tensile strength of lap splices in reinforced concrete members", [M.Sc thesis], West Lafayette, USA Purdue University, p. 165.
[17] ASTM, 2010, Standard test methods and definitions for mechanical testing of steel products – Annex A9 methods for testing steel reinforcing bars. A370. ASTM West Conshohocken, PA, USA.
[18] Horszczaruk, E.K., (2009), "Hydro-abrasive erosion of high performance fiber-reinforced concrete", Wear Vol.267, pp.110-115.
[19] ASTM, 2010, Standard test method: compressive strength of Cylindrical Concrete Specimens, C39/C39M. ASTM West Conshohocken, PA, USA.
[20] Hwang H, Park H, Yi W., (2017), "Non uniform bond stress distribution model for evaluation of bar development length", ACI Structural Journal, Vol. 114, No.4, pp. 839-849.
[21] Eligehausen R, Popov P, Bertero V., (1983), "Local bond stress-slip relationships of deformed bars under generalized excitations", Earthquake Engineering Research Council Report No. 82/23, University of California, Berkeley, CA, 169 pp.
[22] Tastani S, Pantazopoulou S, (2010), "Direct tension pullout bond test: Experimental results", Journal of Structural Engineering, Vol. 136, No. 6, pp. 731-743.
[23] Joint ACI-ASCE Committee 408. Bond and Development of Straight Reinforcing Bars in Tension (ACI 408R-03). American Concrete Institute, Farmington Hills, MI, 2003, 49 pp.
[24] Darwin D, Tholen M., Idun E., Zuo J., (1996a), "Splice strength of high relative rib area reinforcing bars", ACI Structural Journal, Vol. 93, No. 1, pp. 95-107.
[25] Azizinamini A., Pavel R., Hatfield E., Ghosh S., (2000), "Behavior of lap-spliced reinforcing bars embedded in high-strength concrete", ACI Structural Journal; Vol. 96, No. 5, pp. 826-835.